Interferometer for Dispersive Measurements

S. E. Harris*
Departments of Electrical Engineering and Applied Physics, Ginzton Laboratory, Stanford University, Stanford, California 94305, USA

(Received 19 September 2023; accepted 21 December 2023; published 23 January 2024)

We suggest the use of broadband frequency modulation to construct a novel type of optical interferometer. This interferometer is insensitive to optical phase and allows measurement of the group velocity and group velocity dispersion without the need for short pulse apparatus.

DOI: 10.1103/PhysRevLett.132.043802

This Letter describes a novel optical interferometer that is insensitive to optical phase and allows measurement of the group velocity and group velocity dispersion without the need for short pulse apparatus. As shown in Fig. 1 the interferometer consists of a phase modulator, the sample to be studied, and a second modulator. In prototype operation a single optical frequency is incident on the first modulator that produces a broad phase modulated spectral comb. This comb is incident on the sample and then onto the second modulating crystal. This second modulator is run in antiphase with the first so that without a sample the frequency comb is recompressed back to the initial single frequency. With the length known, the normalized power of the single frequency output is measured as a function of the relative phase of the input and output driving waveforms and yields the group velocity of the sample. No short pulse apparatus is required to predict short pulse behavior. This interferometer is motivated by both the recent advances in the use of thin film $LiNbO_3$ [1,2], as well as conceptual advances in the area of synthetic dimensions. Following Buddhiraju *et al.* [3], one dimension is the array of phase modulators. The second, or synthetic, dimension, is the set of frequencies that are applied to the modulating crystals [4]. This Letter will show, for the ideal case, that with L, V_g, and $T = L/V_g$ as the length, group velocity, and transit time through the sample, and with a peak phase retardation of each modulator of δ, and also assuming that there are Q_1 submodulators in the primary dimension, and Q_2 properly phased frequencies in the synthetic dimension, that the fractional accuracy of the interferometer is $T/\Delta T = L/\Delta L = Vg/|\Delta V_g| \approx \pi Q_1 Q_2 \delta$. Here, measurement of ΔT is primary and measurement of L or V_g requires that the other quantity is known.

As to other techniques that accomplish similar objectives, white light Michelson interferometry where identical path lengths allow the observation of fringes is well developed and followed [5]. There is also considerable success with intensity based fiber optic sensors [6] and single mode fiber systems [7].

In the following we follow Zhang *et al.* [8], Raymer [9], and Harris and Buscaino [10] and make use of harmonic balance and a Dirac input-output formalism. The input and output optical envelopes are periodic and are described by kets $|a\rangle$ and $|b\rangle$ whose coefficients are the terms of the Fourier series describing the envelope waveforms $a(t)$ and $b(t)$. The coefficients of $a_n = \langle n|a\rangle$ and $b_n = \langle n|b\rangle$ extend from $-N_m$ to $+N_m$ so that, for example, $b(t) = \sum_{n=-N_m}^{N_m} b_n \exp[in\omega_m t]$.

We allow both the input and output phase modulators of Fig. 1 to be driven by multiple frequencies ω_m and harmonics of ω_m with the constraint that each harmonic component at the input modulator is balanced by an antiphased component at the output modulator. The modulating crystals are assumed to be sufficiently thin that the applied multifrequency electric field (shown for three frequencies) causes an instantaneous variation of phase of

$$\phi(t) = \delta_1 \cos(\omega_m t + \phi_1) + \delta_2 \cos(2\omega_m t + \phi_2) + \delta_3 \cos(3\omega_m t + \phi_3). \quad (1)$$

In the time domain the input and output envelopes are related by $b(t) = \exp[i\phi(t)]a(t)$. We move to the frequency domain by harmonically balancing and using $\exp\{i\delta[\cos(\omega_m t + \phi)]\} = \sum_{q=-\infty}^{+\infty} i^q J_q(\delta) \exp[iq(\omega_m t + \phi)]$. The input and output fields are then related by $|b\rangle = M|a\rangle$ where the matrix elements of the multifrequency modulator are

FIG. 1. Monochromatic light $|a\rangle$ is incident onto a phase modulator, the sample, and a second phase modulator driven 180° out of phase with the first. An output filter passes the incident monochromatic frequency.

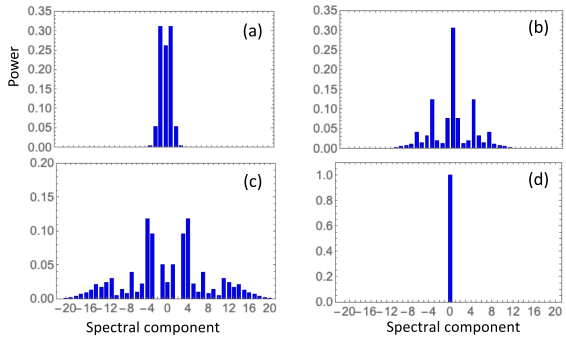

FIG. 2. Modulator power spectrum at a phase retardation of $\delta = 1.5$ rad for each modulator. (a) Input modulator driven at ω_m. (b) Input modulator driven at ω_m, $2\omega_m$, and $3\omega_m$, all with the same phase and no output modulator. (c) Input and output modulators each driven at ω_m, $2\omega_m$, and $3\omega_m$ all with the same phase. (d) Input and output modulators each driven with three frequencies all 180° out of phase from those at the input modulator.

$$M_{nr} = \langle n|M|r\rangle = \sum_h \sum_p i^{(q+h+p)} J_q(\delta_1) J_h(\delta_2) J_p(\delta_3) \times \exp[i(q\phi_1 + h\phi_2 + p\phi_3)], \quad (2)$$

where $q = n - 2h - 3p - r$ and the sums on h and p are over $-N_m$ to $+N_m$. Equations (1) and (2) may be extended to include additional driving harmonics. The matrices of Eq. (2), in the limit of sufficiently large N_m, are unitary and commute with each other. For a sinusoidal drive at only $q\omega_m$, M_{nr} reduces to

$$M_{nr} = i^{(n-r)/q} J_{(n-r)/q}(\delta_q) \exp[i(n-r)/q\phi_q], \quad (3)$$

with the constraint that nonzero elements require the quantity $(n-r)/q$ to be an integer. The matrix with elements of Eq. (2) may be factored into single frequency submatrices, or instead, may be constructed by multiplication of the appropriate submatrices. To obtain the matrix elements of the antiphased modulator of Fig. 1, the phases ϕ_1, ϕ_2, and ϕ_3 are replaced by $\phi_1 + \pi$, ϕ_2, $+\pi$, and $\phi_3 + \pi$.

Figure 2 shows the power spectrum of the input and output modulators in the absence of a sample. In each case the phase retardation of the modulators is $\delta = 1.5$ rad and the number of retained sidebands is $2N_m + 1$ where for this figure $N_m = 20$. As noted, depending on the relative phase of the input and output modulators the spectrum width will approximately double, or in antiphase, collapse to a single frequency.

The matrix for envelope propagation in the sample is diagonal and is readily obtained from the slowly varying envelope equation. Starting with

$$\frac{\partial b(z,t)}{\partial z} + \left(\frac{\partial k}{\partial \omega}\right)\frac{\partial b(z,t)}{\partial t} - \frac{i}{2}\left(\frac{\partial^2 k}{\partial \omega^2}\right)\frac{\partial^2 b(z,t)}{\partial t^2} + \alpha b(z,t) = 0, \quad (4)$$

we expand in the frequency components $b_n(z)$, i.e., $b(z,t) = \sum_n b_n(z)\exp(in\omega_m t)$, and solve for these components as a function of z to obtain

$$b_n(L)/b_n(0) = \exp(-\alpha L)\exp\left[-i\left(\frac{n\omega_m L}{V_g} + n^2\omega_m^2\beta'' L/2\right)\right], \quad (5)$$

with L as the sample length, α as the loss coefficient, and with a sample group velocity of $1/V_g = \partial k/\partial\omega$ and dispersive coefficient $\beta'' = \partial^2 k/\partial\omega^2 = -1/V_g^2(dV_g/d\omega)$. The diagonal matrix that relates the output of the sample to the input has elements

$$M_{nr}^{(\mathrm{prop})} = \exp\left[-i\left(\frac{nL\omega_m}{V_g} + \frac{n^2\omega_m^2\beta'' L}{2}\right)\right]\delta_{nr}. \quad (6)$$

The normalization of $b_0(L)$ is to $b_0\exp(-\alpha L)$, i.e., to the field value at the output of the system with the modulator drives turned off.

The basic interferometer of Fig. 1 consists of a phase modulator, the sample, and a second phase modulator. In the absence of a sample, the monochromatic input beam is expanded by the input modulator and collapsed by the output modulator so as to remain unchanged. With a sample present the input and output fields are related by $|b\rangle = M^{(\mathrm{out})}M^{(\mathrm{prop})}M^{(\mathrm{in})}|a\rangle$ and the monochromatic optical field following the output filter is

$$\langle 0|b\rangle = \langle 0|M^{(\mathrm{out})}M^{(\mathrm{prop})}M^{(\mathrm{in})}|0\rangle = \sum_h\sum_k \langle 0|M^{(\mathrm{out})}|h\rangle\langle h|M^{(\mathrm{prop})}|k\rangle\langle k|M^{(\mathrm{in})}|0\rangle. \quad (7)$$

Though we will return to Eq. (7) for numerical work, first, in order to obtain an analytic expression, we assume a single frequency input ω_m with the same modulation depth δ at both the input and output modulators, and also temporarily neglect group velocity dispersion ($\beta'' = 0$). For a single frequency drive at ω_m, the pertinent matrix elements are

$$\begin{aligned}\langle k|M^{(\mathrm{in})}|0\rangle &= i^k J_k(\delta_{\mathrm{in}})\exp(ik\phi_{\mathrm{in}})\\ \langle h|M^{(\mathrm{prop})}|k\rangle &= \exp(-i\theta_h)\delta_{kh}\\ \langle 0|M^{(\mathrm{out})}|h\rangle &= i^{-h}J_{-h}(\delta_{\mathrm{out}})\exp(-ih\phi_{\mathrm{out}}),\end{aligned} \quad (8)$$

where $\theta_h = (hL\omega_m/V_g) + (h^2\omega_m^2\beta'' L/2)$. We set the relative phase of the input and output modulators to $\phi_{\mathrm{out}} = \phi_{\mathrm{in}} + \pi + \delta\phi$, where $\delta\phi$ is the tunable variable. With $\delta_{\mathrm{in}} = \delta_{\mathrm{out}} = \delta$ the output field is

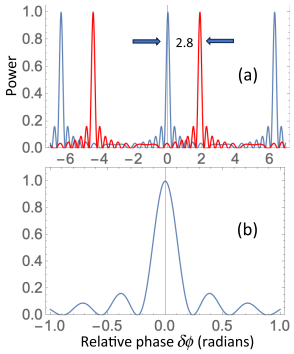

FIG. 3. (a) Interferometer output power versus relative phase $\delta\phi$ between the input and output modulators. The blue curve of part (a) shows the single frequency output power in the absence of a sample. The red curve is with the sample present and is shifted to the right from the blue curve by 2.8 rad. Part (b) shows an enlargement of the blue curve of part (a). In each case the full width at half power of these curves is $2/\delta$ rad, where, here, $\delta = 10$.

$$b_0(L) = \sum_{h=-N_m}^{Nm} J_h(\delta) J_{-h}(\delta) \exp\left[ih\left(\delta\phi - \frac{\omega_m L}{V_g} + \pi\right)\right]. \quad (9)$$

From Eq. (9), using Graf's sum rule the output optical field is

$$b_0(L) = J_0(Z) = J_0\left[\sqrt{2\delta^2(1-\cos(\psi)}\right]$$
$$\psi = \delta\phi - \frac{\omega_m L}{V_g}, \quad (10)$$

where $|b_0(L)|^2$ is the normalized (monochromatic) power transmitted through the output filter.

With the length of the sample known, Eq. (10) is used to measure the group velocity. By first removing the sample, $\delta\phi$ is varied to generate the blue curve of Fig. 3(a). The sample is then inserted to generate the red curve, which, here, is shifted to the right from the blue curve by $\delta\phi = 2.83$ rad. With $L = 3$ cm and $\omega_m = (2\pi)(3 \times 10^9)$, from Eq. (10), the group velocity is $V_g = (\omega_m L/\delta\phi) = c/1.5$. Here, $N_m = 50$.

The attainable accuracy for group velocity measurement is dependent on the width of the curves of Fig. 3(a). Figure 3(b) shows an enlargement of the blue curve. For Z, [Eq. (10)], small enough so that $J_0(Z)$ may be approximated by $1 - Z^2/2$ the full width at half power of each of the curves of Fig. 3 is $2/\delta$ rad. Noting the repetitions of $|b_0|^2$ at intervals of 2π, the number of resolvable data points without repetition is $\pi\delta$. To avoid repetitions the maximum sample length should be less than $L_{\max} = 2\pi V_g/\omega_m$ m, which for this example is $L_{\max} = 6.7$ cm. Equivalently, the maximum delay time that is free of repetitions is $T_{\max} = 2\pi/\omega_m$. Note that the number of resolvable data points in this range $\pi\delta$ is independent of ω_m.

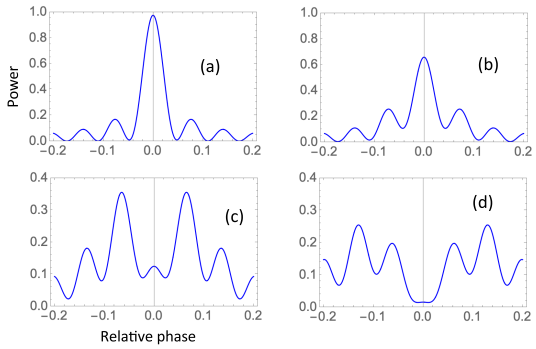

FIG. 4. Interferometer response in the temporal near and far fields. (a) $L = L_{\rm nf}/4$, (b) $L = L_{\rm nf}$, (c) $L = 2L_{\rm nf}$, (d) $L = 3L_{\rm nf}$, where $L_{\rm nf} = 7.2$ m and other parameters are $\omega_m = (2\pi) \times 10$ GHz, $\delta = 50$, $N_m = 100$, and $\beta'' = 50$ ps^2/km.

With the group velocity determined it is often convenient to set the phase difference of the input and output modulating fields to $\delta\phi = \pi + \omega_m L/V_g$. The red curve of Fig. 3(a) will then center at the origin, with group delay no longer playing a role. This choice of relative modulator phase is equivalent to transforming Eq. (4) to local time $\tau = t - L/V_g$.

When working in the time domain, the measurement of group velocity requires that the sample length be sufficiently short that group velocity dispersion plays a negligible role. Conversely the measurement of group-velocity dispersion (GVD) requires that the sample is sufficiently long that GVD dominates. For a Gaussian pulse with a width τ, the temporal near-field length is $L_{\rm nf} = \tau^2/(4ln(2)\beta'')$. For typical fiber parameters and a 1 ps-long pulse, the near-field temporal length in the red region of the spectrum is about 14 m. Working in the frequency domain we replace τ with the inverse bandwidth of the frequency modulated signal $\pi/(\omega_m\delta)$ and test the resulting definition $L_{\rm nf} = [\pi^2/4\ln(2)](1/\omega_m^2\beta''\delta^2)$. Returning to Eqs. (2) and (7), Fig. 4 shows a plot of the output power $|b_0|^2$ versus relative modulator phase for four different values of the ratio $L/L_{\rm nf}$. When the sample is short as compared to $L_{\rm nf}$ we obtain a similar curve as in Fig. 3(b). When the sample length equals and exceeds $L_{\rm nf}$ the normalized power at zero relative phase declines toward zero, and this variance may be used to measure β''. [If a tunable monochromatic laser source is available the group velocity may also be measured by the more straight forward method of Fig. (3).]

To increase the fractional resolution of the interferometer we follow Lončar, Fan, and Hu and use what is termed "synthetic variables" [1–4]. For both the input and output modulators there are two dimensions: the primary dimension that delineates the set of submodulators, and

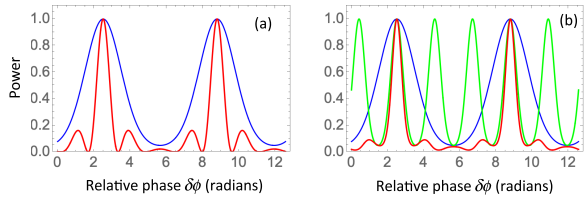

FIG. 5. Primary (a) and synthetic dimension (b). Part (a) shows the output power for an applied single frequency modulator (blue) and for three cascaded modulators (red). Part (b) shows the output power for an applied single frequency (blue), an applied third harmonic (green), and a single modulator with the three harmonics simultaneously applied (red). Both dimensions, though for different reasons, yield the same increase in resolution $T/\Delta T$ of a factor of 3 (see text).

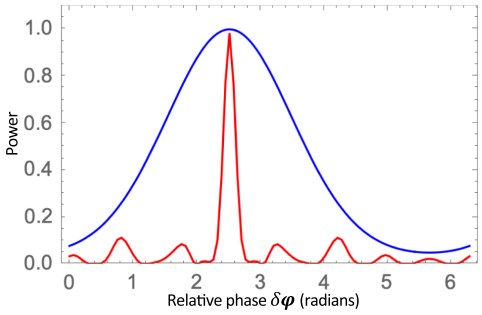

FIG. 6. Interferometer with a single modulator at the input and an antiphased modulator at the output, both with $\delta = 1$ (blue curve), and three in-line modulator components with three harmonics applied to each (red curve). The resolution of the red curve as compared to the blue curve (half power) is increased by a factor of 9.

the synthetic dimension that delineates the set of phased harmonic frequencies that are simultaneously applied to each submodulator. We choose the phases of the three applied harmonics at frequencies $(\omega_m, 2\omega_m, 3\omega_m)$ to be $(\phi_m, 2\phi_m, 3\phi_m)$ so that the applied waveform is a periodic pulselike three term Fourier series. Relative phase, in all figures and text, is the phase difference between the input and output modulators, as measured *at the fundamental frequency*. Results are numerical and are based on Eqs. (1), (2), (6), and (7).

We observe some properties of the matrices of Eq. (2). (1) In the primary dimension if each of three component modulators has a peak phase δ, the total modulator will have an argument of 3δ. It is an engineering choice as to whether to make a higher voltage modulator, or instead, use a sequence of three lower voltage modulators. (2) By applying the sum of phased modulation frequencies (synthetic dimension) we decrease the repetition frequency of power peaks versus relative phase. This is a consequence of a phased (three term) Fourier series with terms of equal amplitude. Such a waveform has a resolution determined by its highest frequency component and a repetition frequency determined by its lowest frequency component. These properties are demonstrated in Fig. 5. Part (a) shows the effect of cascading three primary modulators all driven at the same frequency ω_m. Part (b) contrasts a single modulator running at the third harmonic alone (green), with a single modulator driven by three harmonics (red).

Figure 6 shows the interplay of the two dimensions with three modulators in a row, each with three frequencies applied. The resolution, red compared to blue, is now increased by a factor of 9. This figure uses Eqs. (2) and (7), including GVD, with parameters $\delta = 1.0$, $L = 2.66$ cm, $\omega_m = (2\pi)(3 \times 10^9)$, $V_g = c/1.5$, $L_{\max} = 0.066$ m, $\beta'' = 25$ ps^2/km, and $N_m = 18$.

The Supplemental Material [11] describes a time domain treatment that is complimentary to the frequency domain treatment of the primary text. With GVD neglected, the time domain approach is intuitive and concise. It is shown, as a special case, how using only the fundamental and the tenth harmonic, that the essential features of measurement of ΔT at an accuracy of the inverse bandwidth of the highest harmonic, together with a repetition frequency of the fundamental is retained.

The author thanks Shanhui Fan, Moti Segev, Joseph Kahn, and Brandon Buscaino for inspiring discussions.

*Corresponding author: seharris@stanford.edu

[1] C. Wang, M. Zhang, X. Chen, M. Bertrand, A. Shams-Ansari, S. Chandrasekhar, P. Winzer, and M. Lončar, Integrated lithium niobate electro-optic modulators operating at CMOS-compatible voltages, Nature (London) **562**, 101 (2018).

[2] Graham Reed, David Thomson, Weiwei Zhang, Frederic Gardes, Lorenzo Mastronardi, Ke Li, Shinji Matsuo, Shigeru Kanazawa, Laurent Vivien, Christian Lafforgue, John E. Bowers, Christian Koos, Romagnoli, Marko Lončar, Mian Zhang, Stefan Abel, and Ling Liao, *Integrated Photonics for Data Communication Applications* (Elsevier, New York, 2023), pp. 69–121.

[3] Siddharth Buddhiraju, Avik Dutt, Momchil Minkov, Ian A. D. Williamson, and Shanhui Fan, Arbitrary linear transformations for photons in the frequency synthetic dimension, Nat. Commun. **12**, 2401 (2021).

[4] Yaowen Hu, Christian Reimer, Amirhassan Shams-Ansari, Mian Zhang, and Marko Loncar, Realization of high dimensional frequency crystals in electro-optic microcombs, Optica **7**, 1189 (2020).

[5] S. Diddams and J.-C. Diels, Dispersion measurements with white-light interferometry, J. Opt. Soc. Am. B **13**, 1120 (1996).

[6] A. Wang, H. Xiao, J. Wang, Z. Wang, W. Zhao, and R. G. May, Self-calibrated interferometric-intensity-based optical fiber sensors, J. Lightwave Technol. **19**, 1495 (2001).

[7] Daulet Askarov, Bogdan Szafraniec, Douglas M. Baney, and Joseph M. Kahn, Frequency-derivative measurement technique for dispersive effects in single-mode fiber systems, J. Lightwave Technol. **32**, 4456 (2014).

[8] M. Zhang, B. Buscaino, C. Wang, A. Shams-Ansari, C. Reimer, R. Zhu, J. M. Kahn, and M. Lončar, Broadband electro-optic frequency comb generation in a lithium niobate microring resonator, Nature (London) **568**, 373 (2019).

[9] M. G. Raymer and C. J. McKinstrie, Quantum input-output theory for optical cavities with arbitrary coupling strength: Application to two-photon wave-packet shaping, Phys. Rev. A **88**, 043819 (2013).

[10] S. E. Harris and B. Buscaino, Technique for generating broadband FM light, Opt. Lett. **45**, 2058 (2020).

[11] See Supplemental Material at http://link.aps.org/supplemental/10.1103/PhysRevLett.132.043802 for complete details.